Supporting Information

Lu et al. 10.1073/pnas.1322357111

Experimental Procedures

Expression and Purification of Serum Amyloid A 1 and Maltose Binding Protein-Serum Amyloid A 1_{89} Fusion Proteins. Mature human serum amyloid A (SAA)1.1 peptide (residues 1–104) (Gene ID code NM_199161; hereafter SAA1) was cloned into a pET30a vector between the NdeI and XhoI sites with ($_{his6}$SAA1) or without (SAA1) an N-terminal histidine (his_6) tag and expressed at 25 or 30 °C as a soluble protein in the BL21 strain of *Escherichia coli* and purified by either a HisTrap HP column (GE Healthcare) or a DEAE column and gel-filtration column in the presence of 4 N guanidine as previously described (1, 2). Selenomethionine-labeled SAA1 protein was expressed in the *E. coli* B834 strain (Novagen) using the nontagged construct in selenomethionine-supplemented minimal medium M9 and purified similar to the native protein. All proteins were further purified using a Superdex 200 gel-filtration column before crystallization. Attempts to purify a soluble C-terminal 15-residue truncate of SAA1 failed due to the formation of inclusion bodies in *E. coli*. Therefore, this SAA fragment, residues 1–89, was expressed at 18 °C in a soluble form fused to maltose binding protein (MBP) using pMAL-p5g vectors between the SnabI and XhoI sites with a C-terminal his_6 tag (designated MBP-$SAA1_{89}$). MBP-$SAA1_{89}$ proteins were purified by using HisTrap HP and Superdex 200 columns (GE Healthcare) as described for $_{his6}$SAA1. All SAA mutations were generated using a QuikChange Mutagenesis Kit (Qiagen) and expressed and purified similar to the wild type.

Crystallization and Structure Determination. The non–his_6-tagged SAA1 and its selenomethionine derivative were crystallized in 2.0 M $(NH_4)_2SO_4$, 0.1 M Hepes (pH 7.5), and 6% (wt/vol) PEG 400 in orthorhombic space group $P2_12_12$ and diffracted to 2.2-Å resolution. The crystals for $_{his6}$SAA1 were grown in 30% (wt/vol) PEG 2000 monomethyl ether, 0.1 M Tris (pH 8.5), and 0.2 M trimethylamine *N*-oxide in the rhombohedral space group R32 and diffracted to 2.5-Å resolution. All X-ray data were collected at Southeast Regional Collaborative Access Team beamlines and processed with HKL2000 (3) (Table S1). The structure of SAA1 was initially determined by multiwavelength anomalous dispersion using a selenomethionine derivative for the orthorhombic crystal form using autoSHARP with an overall mean anomalous phasing power of 1.26 and figure of merit of 0.74 (4) (Global Phasing) and ARP/wARP (5) and refined with REFMAC5 (6) and PHENIX (7). The structure of SAA1 in the R32 crystal form was subsequently determined by a molecular replacement method using Phaser (8) and refined with autoBUSTER (9) with repeated cycles of rebuilding in Coot (10). Data collection and model statistics are summarized in Table S1. Figures were prepared with PyMOL (www.pymol.org) (11).

Analytical Ultracentrifugation. Sedimentation velocity data were collected in a Beckman Coulter XL-A centrifuge. $_{his6}$SAA1 (0.02–0.82 mg/mL), SAA1 (0.03–0.3 mg/mL), or MBP-$SAA1_{89}$ (0.06–0.7 mg/mL) in 10 mM Hepes (pH 7.4) and 0.15 M NaCl was loaded in a double-sector cell and data were collected at 50,000 rpm using an absorbance detection wavelength of 280 nm at 20 °C. The raw sedimentation velocity absorbance profiles were analyzed by SEDFIT using a continuous [c(s)] distribution model to obtain the apparent distribution of sedimentation coefficients (s) (11). The sedimentation equilibrium distributions of $_{his6}$SAA1 (0.02–0.2 mg/mL) and refolded SAA1 were monitored using absorbance detection at 280 and 260 nm at three rotor speeds (6, 9, and 15 krpm) at 4 °C. The data were globally fitted by SEDPHAT using the model of species analysis with mass conservation constraints with 95% confidence (11). The goodness of fit was assessed by the quality of the residuals within a local rmsd of 0.005.

Thioflavin T Fluorescence. Fluorescence measurements were performed as described previously (12) at 25 or 37 °C in 96-well plates on a Synergy H1 hybrid reader (BioTek) with an excitation wavelength of 430 nm. The final thioflavin T (ThT) concentration was 10 μM in 20 mM Hepes (pH 7.5) and 0.15 M NaCl. To test the propensity of amyloid fibril formation, individual peptides, including helix 1 (residues 1–26), helix 2-short (residues 32–40), helix 2-long (residues 32–48), helix 3 (residues 50–71), and helix 4 (residues 73–88), were synthesized (GenScript) and resuspended at a concentration of 50 μg/mL, and ThT fluorescence intensity was monitored at 37 °C for 36 h without preincubation. The cathepsin digestion of $_{his6}$SAA1 protein at 0.4 mg/mL was carried out at 37 °C in 50 μM sodium acetate (pH 5.2), 10 μM ThT, 10 mM EDTA, 5 mM DTT, and 0.15 M NaCl supplemented with 2 units of cathepsin (Sigma-Aldrich). The ThT fluorescence intensity of MBP-$SAA1_{89}$ samples was measured at 25 °C.

Congo Red Binding. Congo red (CR) binding was detected using a previously described method (13) in 96-well plates. SAA1 or control proteins were incubated with 15 μM CR at 37 °C for 2 h in 20 mM Hepes (pH 7.5) and 0.15 M NaCl.

Negative-Staining Electron Microscopy. EM grids of negatively stained samples were prepared as previously described (14). Negatively stained EM grids were observed on a Tecnai T20 microscope (FEI) operated at 120 kV. Images were recorded at a nominal magnification of 50,000× using a 4K × 4K CCD camera (Gatan; UltraScan 4000), corresponding to a pixel size of 2.1 Å per pixel (T20) on the specimen. Defocuses were set to −1.5 μm. Actual defocus values were determined for each micrograph using CTFFIND (15) and ranged from −1.5 to −2 μm; 2,886 $_{his6}$SAA1 protein particles were selected manually from 50 images. Individual particles were windowed out from the raw images and subjected to five cycles of ultireference alignment and K-means classification using SPIDER (16).

Image recording for MBP-$SAA1_{89}$ fusion proteins was carried out similar to as described above; 1,962 particles were manually picked from 68 raw images. These particles were classified into 64 2D averages using the K-means classification algorithm implemented in EMAN2 (17).

Surface Plasmon Resonance Experiments. Surface plasmon resonance measurements were performed using a Biacore 3000 instrument and analyzed with BIAevaluation 4.1 software (Biacore). Biotinylated heparin was obtained from Sigma-Aldrich. A monomeric form of recombinant human SAA was purchased from PeproTech. To measure the affinity to human SAA1 and mutants, biotinylated heparin was immobilized on streptavidin chips (Biacore) to 100–400 response units (RUs). The analytes consisted of serial dilutions of SAA1 samples as stated in a buffer containing 10 mM Hepes (pH 7.4) and 0.15 M NaCl. The affinity was calculated using steady-state fitting. The ELISA on the interaction of heparin with human SAA1 and mutants was carried out using an SAA human ELISA kit (Invitrogen) according to the manufacturer's instructions. In the ELISAs on the binding of SAA proteins to high-density lipoprotein (HDL), anti-HDL antibody (clone 1C5; Abcam) was coated on plates and then HDL (RayBiotech) at 100 μg/mL was captured. To test HDL

binding, SAA proteins at different concentrations were added and then bound SAA was detected by anti-SAA antibodies (sc-20651; Santa Cruz Biotechnology) followed by an HRP-conjugated anti-rabbit antibody (Cell Signaling).

1. Wang L, Lashuel HA, Walz T, Colon W (2002) Murine apolipoprotein serum amyloid A in solution forms a hexamer containing a central channel. *Proc Natl Acad Sci USA* 99 (25):15947–15952.
2. Yamada T, Kluve-Beckerman B, Liepnieks JJ, Benson MD (1994) Fibril formation from recombinant human serum amyloid A. *Biochim Biophys Acta* 1226(3):323–329.
3. Otwinowski ZMW (1997) Processing of X-ray diffraction data collected in oscillation mode. *Methods Enzymol* 276:307–326.
4. Bricogne G, Vonrhein C, Flensburg C, Schiltz M, Paciorek W (2003) Generation, representation and flow of phase information in structure determination: Recent developments in and around SHARP 2.0. *Acta Crystallogr D Biol Crystallogr* 59(Pt 11): 2023–2030.
5. Langer G, Cohen SX, Lamzin VS, Perrakis A (2008) Automated macromolecular model building for X-ray crystallography using ARP/wARP version 7. *Nat Protoc* 3(7): 1171–1179.
6. Murshudov GN, et al. (2011) REFMAC5 for the refinement of macromolecular crystal structures. *Acta Crystallogr D Biol Crystallogr* 67(Pt 4):355–367.
7. Adams PD, et al. (2002) PHENIX: Building new software for automated crystallographic structure determination. *Acta Crystallogr D Biol Crystallogr* 58(Pt 11):1948–1954.
8. McCoy AJ, et al. (2007) Phaser crystallographic software. *J Appl Crystallogr* 40(Pt 4): 658–674.
9. Blanc E, et al. (2004) Refinement of severely incomplete structures with maximum likelihood in BUSTER-TNT. *Acta Crystallogr D Biol Crystallogr* 60(Pt 12 Pt 1):2210–2221.
10. Emsley P, Lohkamp B, Scott WG, Cowtan K (2010) Features and development of Coot. *Acta Crystallogr D Biol Crystallogr* 66(Pt 4):486–501.
11. Brown PH, Schuck P (2008) A new adaptive grid-size algorithm for the simulation of sedimentation velocity profiles in analytical ultracentrifugation. *Comput Phys Commun* 178(2):105–120.
12. LeVine H III (1999) Quantification of beta-sheet amyloid fibril structures with thioflavin T. *Methods Enzymol* 309:274–284.
13. Thompson MJ, et al. (2006) The 3D profile method for identifying fibril-forming segments of proteins. *Proc Natl Acad Sci USA* 103(11):4074–4078.
14. Ohi M, Li Y, Cheng Y, Walz T (2004) Negative staining and image classification—Powerful tools in modern electron microscopy. *Biol Proced Online* 6:23–34.
15. Mindell JA, Grigorieff N (2003) Accurate determination of local defocus and specimen tilt in electron microscopy. *J Struct Biol* 142(3):334–347.
16. Frank J, et al. (1996) SPIDER and WEB: Processing and visualization of images in 3D electron microscopy and related fields. *J Struct Biol* 116(1):190–199.
17. Tang G, et al. (2007) EMAN2: an extensible image processing suite for electron microscopy. *Journal of structural biology* 157(1):38–46.

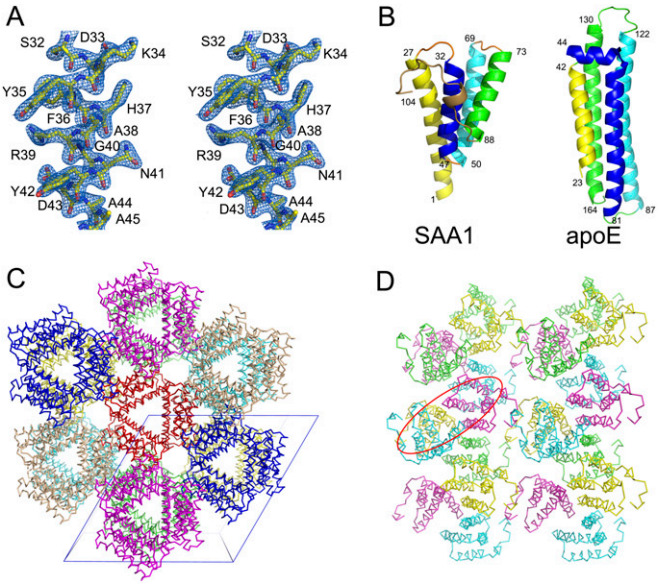

Fig. S1. (*A*) Close-up view of residues 32–44 and their ($2F_o - F_c$) electron density map contoured at 1.0σ. (*B*) SAA1.1 and ApoE monomer structures adopt a different four-helix bundle topology. (*C*) $_{his6}$SAA1 crystal lattice in a trigonal space group with the unit cell boundary indicated. (*D*) Refolded SAA1 crystal lattice in an orthorhombic space group. There is one twofold symmetry in the $P2_12_12$ crystal; the cyan and purple monomers are highlighted in a red oval. This is a different twofold symmetry from that observed in the hexameric SAA. The twofold interface is smaller and involves a third SAA monomer (colored in yellow).

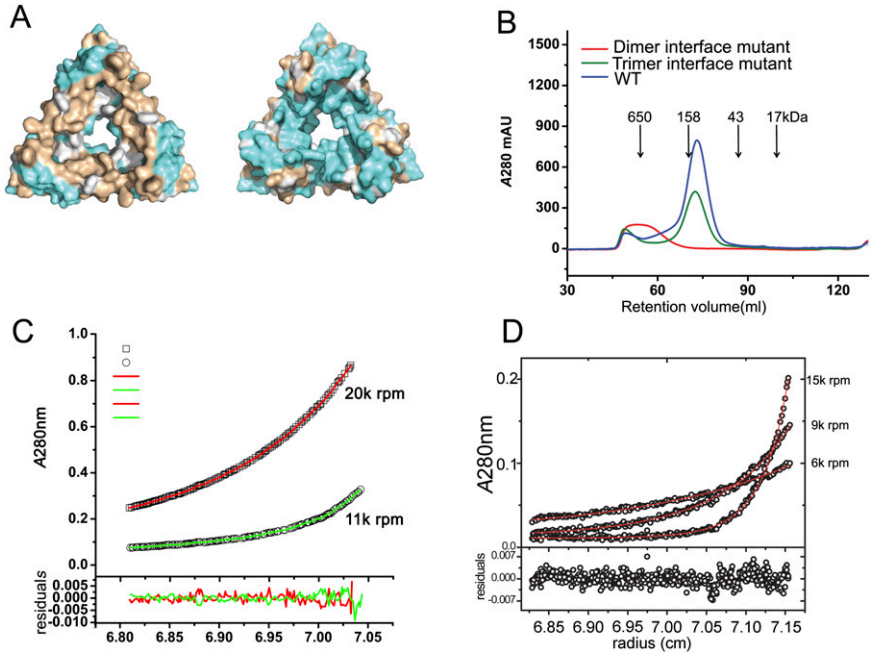

Fig. S2. (*A*) The polar (marine) and hydrophobic (wheat) property of the two triangle surfaces on each SAA1 trimer. (*B*) Effects of SAA1.1 mutations on the oligomerization state. (*C* and *D*) Equilibrium sedimentation AUC analysis of refolded SAA1.1 (*C*) and native $_{his6}$SAA1 (*D*). Solid lines represent the global fit of typical traces at different speed. The *Lower* panel shows the residuals for each fit.

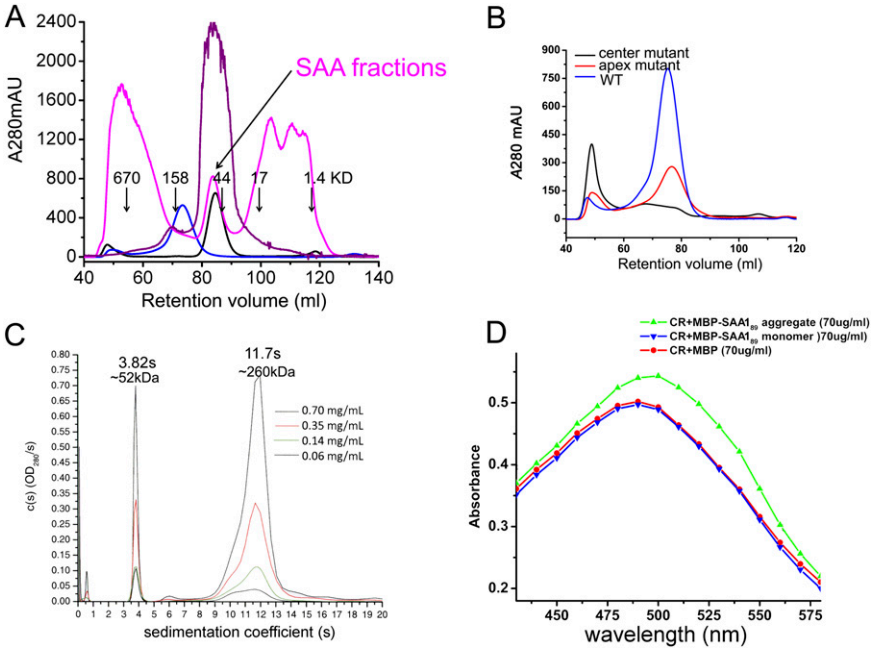

Fig. S3. Characterization of SAA1.1 proteins. (*A*) Superimposed gel filtration profiles of native $_{his6}$SAA1 in the absence of 4M GnHCl (blue line), $_{his6}$SAA1 in the presence of 4M GnHCl (black line), refolded SAA1 in the absence of 4M GnHCl (purple line), and refolded SAA1 in the presence of 4M GnHCl during the gel-filtration purification step (magenta line). The nearly pure SAA1 fractions were indicated by an arrow, which showed the same apparent molecular weight as refolded SAA1 in the absence of 4M GnHCl. The protein concentration was monitored by absorbance in milliabsorbance units (mAU) at 280nm. (*B*) gel-filtration chromatography profile of $_{his6}$SAA1 wild type, center pore mutant and apex mutant. (*C*) Sedimentation velocity AUC profile of MBP-SAA1$_{89}$ truncate. (*D*) Absorption spectra of congo-red (CR) in the presence of MBP-SAA1$_{89}$ aggregate (green), MBP-SAA1$_{89}$ monomer (blue), and MBP (red).

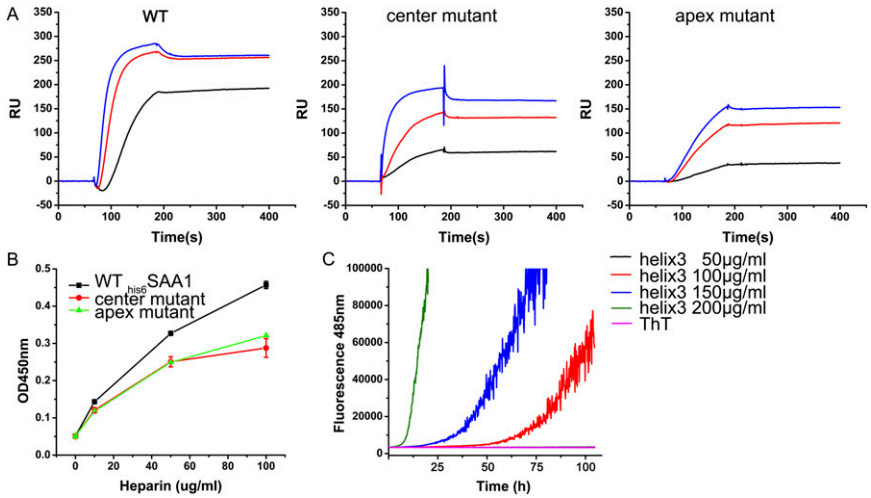

Fig. S4. Interaction of $_{his6}$SAA1 hexamer and mutants with heparin. (*A*) Surface plasmon resonance analysis with biotinylated heparin immobilized on streptavidin chips. The sensorgrams are staggered in the order of the indicated analyte concentrations (nM). (*B*) ELISA analysis with SAA1 proteins coated on the plates. (*C*) ThT binding shows that helix 3 peptide forms amyloid at higher concentrations. The error bars are SDs of three experiments.

Table S1. Data collection and refinement statistics

	SAA1			$_{his6}$SAA1
Data collection	Native	SeMet (Se peak)	SeMet (Se edge)	Native
Space group	$P2_12_12$	$P2_12_12$	$P2_12_12$	R32
Wavelength, Å	1.00	0.9787	0.9796	1.00
Unit-cell dimension, Å	a = 68.6, b = 128.4, c = 50.2	a = 69.0, b = 127.9, c = 50.3	a = 68.9, b = 128.7, c = 50.5	a = b = 93.9, c = 130.5
Resolution range, Å	50.0–2.19 (2.30–2.19)	50.0–2.42 (2.48–2.42)	50.0–2.50 (2.54–2.50)	20.0–2.50 (2.54–2.50)
Unique reflections	22,939 (1,413)	17,734 (1,152)	16,207 (730)	7,791 (376)
Average redundancy	9.9 (6.9)	24.9 (21.6)	13.4 (9.1)	6.4 (3.2)
R_{sym}, %*	9.8 (48.9)	14.2 (54.9)	13.0 (60.5)	10.2 (51.1)
I/σ(I)	24.4 (2.8)	22.2 (7.0)	18.7 (2.1)	16.2 (3.0)
Completeness, %	98.3 (92.6)	99.7 (99.8)	99.2 (90.6)	99.8 (99.7)
Refinement statistics				
Refinement resolution, Å		46.7–2.19 (2.29–2.19)		18.5–2.50 (2.79–2.50)
R_{cryst}, %†		20.4 (26.2)		24.9 (26.0)
R_{free}, %‡		25.6 (33.5)		25.8 (30.8)
Protein atoms		3,348		1,658
Waters and ligands		101× H_2O, 11× PEG, 4× sulfate,		6× H_2O, 6× PEG
Rmsd from ideal values				
Bond length, Å		0.003		0.008
Bond angle, °		0.67		0.86
Mean B factor, Å^2		36.2		82.5
Wilson plot B factor, Å^2		36.8		71.1
Ramachandran statistics				
Most favored region, %		99.5		97.5
Additionally allowed, %		0.5		2.5

Values in parentheses represent data for the highest-resolution shell.

*$R_{sym} = \sum_h\sum_i|I_i(hkl) - <I(hkl)>|/\sum_h\sum_i I_i(hkl)$.

†$R_{cryst} = \sum||F_o| - |F_c||/\sum|F_o|$ calculated from the working dataset.

‡R_{free} is calculated from 5.17 and 9.68% of data randomly chosen not to be included in refinement for crystal forms I and II, respectively.